

Nuclear Reactions Governing the Nucleosynthesis of ^{44}Ti

The, L.-S., Clayton, D. D., Jin, L., & Meyer, B. S.

Department of Physics & Astronomy, Clemson University, Clemson, SC 29634-1911

ABSTRACT

Large excesses of ^{44}Ca in certain presolar graphite and silicon carbide grains give strong evidence for ^{44}Ti production in supernovae. Furthermore, recent detection of the ^{44}Ti γ -line from the Cas A SNR by CGRO/COMPTEL shows that radioactive ^{44}Ti is produced in supernovae. These make the ^{44}Ti abundance an observable diagnostic of supernovae.

Through use of a nuclear reaction network, we have systematically varied reaction rates and groups of reaction rates to experimentally identify those that govern ^{44}Ti abundance in core-collapse supernova nucleosynthesis. We survey the nuclear-rate dependence by repeated calculations of the identical adiabatic expansion, with peak temperature and density chosen to be $5.5 \times 10^9 \text{ K}$ and 10^7 g cm^{-3} , respectively, to approximate the conditions in detailed supernova models. We find that, for equal total numbers of neutrons and protons ($\eta=0$), ^{44}Ti production is most sensitive to the following reaction rates: $^{44}\text{Ti}(\alpha, p)^{47}\text{V}$, $\alpha(2\alpha, \gamma)^{12}\text{C}$, $^{44}\text{Ti}(\alpha, \gamma)^{48}\text{Cr}$, $^{45}\text{V}(p, \gamma)^{46}\text{Cr}$. We tabulate the most sensitive reactions in order of their importance to the ^{44}Ti production near the standard values of currently accepted cross-sections, at both reduced reaction rate ($0.01 \times$) and at increased reaction rate ($100 \times$) relative to their standard values. Although most reactions retain their importance for $\eta > 0$, that of $^{45}\text{V}(p, \gamma)^{46}\text{Cr}$ drops rapidly for $\eta \geq 0.0004$. Other reactions assume greater significance at greater neutron excess: $^{12}\text{C}(\alpha, \gamma)^{16}\text{O}$, $^{40}\text{Ca}(\alpha, \gamma)^{44}\text{Ti}$, $^{27}\text{Al}(\alpha, n)^{30}\text{P}$, $^{30}\text{Si}(\alpha, n)^{33}\text{S}$. Because many of these rates are unknown experimentally, our results suggest the most important targets for future cross section measurements governing the value of this observable abundance.

Subject headings: nuclear reactions, nucleosynthesis, abundances

1. INTRODUCTION

Radioactive ^{44}Ti , produced in core collapse supernovae, is an isotope of extraordinary astrophysical significance. Its primary observable effects appear to be three in number and will likely grow in coming years. The first is that the relatively large abundance of ^{44}Ca —it is the second most abundant calcium isotope and the 44th most abundant species overall in solar system material—is overwhelmingly due to its synthesis as ^{44}Ti parent (Bodansky, Clayton, & Fowler 1968; Woosley, Arnett, & Clayton 1973; Timmes et al. 1996). The second is that resulting gamma rays from young core collapse supernovae are expected to be visible from several Galactic remnants (Clayton 1971; Hartmann et al. 1993; Leising & Share 1994; Dupraz et al. 1997). ^{44}Ti decays to ^{44}Sc emitting 67.9 keV (100%) and 78.4 keV (98%) lines. ^{44}Sc then decays into ^{44}Ca , which emits a 1.157 MeV (100%) line. The search for Galactic ^{44}Ti gamma-ray lines has been carried out by both the gamma-ray spectroscopy experiments on HEAO 3 (Mahoney et al. 1992), the SMM satellite (Leising & Share 1994), and by CGRO surveys with COMPTEL (Dupraz et al. 1997). Only from the direction of Cas A SNR has the 1.157 MeV ^{44}Ti gamma line flux been detected by COMPTEL (Iyudin et al. 1994; The et al. 1995), with a flux initially reported at $(7.0 \pm 1.7) \times 10^{-5} \gamma \text{ cm}^{-2} \text{ s}^{-1}$. Subsequently Iyudin et al. (1997) have reported CGRO cycle 1-5 results from a $2 \times 10^6 \text{ s}$ exposure of Cas A. The result is a flux of $(4.8 \pm 0.9) \times 10^{-5} \gamma \text{ cm}^{-2} \text{ s}^{-1}$ and significance of detection of 6σ . This measurement is reasonably consistent with the CGRO/OSSE three-line flux measurements (The et al. 1996) of $(1.8 \pm 1.5) \times 10^{-5} \gamma \text{ cm}^{-2} \text{ s}^{-1}$ and with the preliminary result of RXTE/HEXTE AO1 & AO2 observations (Rothschild et al. 1998) of $(1.3 \pm 1.2) \times 10^{-5} \gamma \text{ cm}^{-2} \text{ s}^{-1}$, at 4% confidence level with the most probable flux of the combined three instrument measurements being $3.2 \times 10^{-5} \gamma \text{ cm}^{-2} \text{ s}^{-1}$. This flux translates into $(1.3, 7.8) \times 10^{-4} M_{\odot}$ of ^{44}Ti for a ^{44}Ti half-life of (66.6, 39.0) yrs respectively (Alburger & Harbottle 1990; Meissner 1996), distance of 3.4 kpc to Cas A (Reed et al. 1995) and age of 315 yrs (Ashworth 1980). Because the ^{44}Ti yield probes the dynamics of core collapse supernova nucleosynthesis, and in particular, the location of the mass cut, the pre-supernova composition inside $\sim 2 M_{\odot}$, and the maximum temperature and density reached during the passage of the shock wave in the ejecta, this detection has generated great enthusiasm for SNR distance measurements (Reed et al. 1995), for γ -ray line observations (Iyudin et al. 1997; Rothschild et al. 1998; The et al. 1996), for new nuclear laboratory experiments to accurately determine the ^{44}Ti half-life (Alburger & Harbottle 1990; Meissner 1996; Norman et al. 1997; Górrres et al. 1998), and for theoretical nucleosynthesis calculations in the context of core-collapse supernovae (Woosley & Hoffman 1991; Timmes et al. 1996; Nagataki et al. 1997).

The third effect is that ^{44}Ca -enriched silicon-carbide particles extracted from meteorites have been identified (Amari et al. 1992; Nittler et al. 1996; Hoppe et al. 1996) as presolar particles that condensed within supernova ejecta during their first few years of expansion, while ^{44}Ti was still at its initial value (Clayton 1975). These grains are of enormous value in probing the dynamics and make up of supernova ejecta (Clayton, Amari, & Zinner 1997).

In the near future, we can expect very accurate ^{44}Ti line flux measurements, precise distances

to several young SNRs, and a accurate ^{44}Ti half-life (recent measurements of ^{44}Ti lifetime by Norman et al. 1997 and Görres et al. 1998 seem to converge at a value of (87.7 ± 1.7) y). This reduction of current uncertainties will allow more meaningful comparisons of the ^{44}Ti mass in Cas A and other young SNRs (in particular, Tycho and Kepler) to supernova models. However, a remaining factor limits such comparisons between observations of ^{44}Ti mass and supernova models, namely, the uncertainty in the nuclear cross sections governing the synthesis of ^{44}Ti . A large number of nuclear reactions play a role in ^{44}Ti production, and the cross sections for many of these are only estimated from nuclear models. While these estimated cross sections should be fairly accurate in many cases (Rauscher, Thielemann, & Kratz 1997), there is no guarantee that they are so, and only laboratory measurements will provide us with confidence in the yield predictions from nucleosynthesis calculations. Cross section values enter linearly into the stellar reaction rate. For this reason, and because of ^{44}Ti ’s astrophysical significance, we have surveyed the relative importance of the nuclear reaction rates that govern its abundance. Our purpose is to identify for the nuclear physics community those reaction rates that have the greatest astrophysical importance to the ^{44}Ti abundance and which, consequently, would be appropriate targets for future cross section measurements. Using a nuclear reaction network with 378 isotopes, we have systematically varied specific reaction rates and groups of reaction rates in an experimental test for astrophysical significance. We identify the most important nuclear rates and explain our understanding of the overall rate dependencies we have found. Preliminary results were presented in Jin et al. (1997). In the following we will refer to the terms “cross section” and “reaction rate” somewhat interchangeably. It should be understood that “reaction rates” are calculated from either theoretically predicted and/or experimentally measured cross sections. Related to this survey is work done by Woosley & Hoffman (1991) in which they varied the peak temperatures, densities, and neutron excesses of explosive silicon burning in alpha-rich freezeout to find the range of ^{57}Co and ^{44}Ti production with standard reaction rates.

2. Overall Strategy

2.1. Laboratory Nuclear Astrophysics

The present work is part of a long-range effort to determine the identity of the nuclear reactions that are of greatest importance to nucleosynthesis in stars. The goal is to improve the accuracy of nucleosynthesis calculations by encouraging experimental study of key reactions. Although this has always been an important part of the science, as embodied for example in the Nobel-Prize winning work of W. A. Fowler, it has not always been emphasized with useful clarity. Most nucleosynthesis calculations have been concerned with testing the fundamental paradigm: does the evolution and explosion of stars reproduce the known elemental and isotopic abundances? Most research efforts address more explicitly the astrophysical models than the nuclear data base. That data base is usually taken as a given, and so most calculations have used the tabulated values as given in order to calculate the nuclear production within specific stellar

models. All have been aware in this that the nuclear data base is uncertain, and conclusions have been drawn that respect that uncertainty. But almost no nucleosynthesis calculations display the dependence of the abundances on the values of the reaction rates used. The community of laboratory nuclear physicists devoted to this problem has continued the work of improving that data base. Indeed the level of interest in this has been increasing in the past few years, in part because of the construction of several new radioactive-ion-beam facilities (Lubkin 1997), each of which has realized that those facilities offer new opportunities to clarify cross sections near the $Z=N$ line in the nuclide chart where several important astrophysical processes occur.

What is often missing is a clear idea of the relative importance of specific reactions for the overall problem. Laboratory scientists quite understandably do not wish to pursue all of the large numbers of reactions that naturally occur. It has always been the demonstrated importance of the exact value for a cross section that has inspired improved measurements of it. This has usually been rather clear in those basic cycles instrumental for nuclear power in stars, where the identity of the important reactions is visible. The important reactions during advanced burning processes responsible for many of the intermediate mass nuclei have not been so closely scrutinized, however. During these processes a large number of reactions occur simultaneously, often presenting parallel paths to the same result, so that the significance of the value of each is obscured. The size of a cross section is no sure guide to the importance of the value attached to it. In certain circumstances during advanced burning a huge reaction rate is often opposed by a huge and nearly equal flow due to the inverse reaction, nullifying importance for the exact value of that reaction rate for that epoch of that process. So complex are those networks that unambiguous responsibility for final abundances has been difficult to assign. This is especially true for nuclear processes taking place in or near equilibrium. Our approach to clarifying this is to explicitly change the value of a specific reaction rate (or rates) and to redo the calculation to test the sensitivity of a final answer to its value. We have developed a logical sequence to do this in a practical manner.

2.2. Four Requirements for Meaningful Measurements

Because the goal is to ultimately influence measurements of key cross sections, it is useful to list explicitly the four requirements that are, at a minimum, needed for this goal to be achieved:

1. An appropriate astrophysical model of events significant for nucleosynthesis;
2. An observable from that process, usually an abundance result that is either known or measurable;
3. Dependency of the value of the observable on the value of a nuclear cross section;
4. Experimental strategy for measuring that cross section, or at least of using measurable data to better calculate it.

It is important to note in item 1 that the model must be “appropriate”, not necessarily “correct”. We know that models of supernovae, for example, are never “correct”. The unknowns from all of physics are many. But the model may be appropriate for testing the sensitivity of the observable to the value of the cross section in question. The cross-section dependence may be determinable with more accuracy than the absolute value of the observable, because the absolute value depends upon the model’s realism. Indeed, the model’s realism will later be tested by the nucleosynthesis results it produces once the important reaction rates are known. We stress this distinction that has confused many who ask, “Why is it so important to pin down the key cross sections when the astrophysical model introduces more uncertainty than the cross sections do?”

The observable will usually be some abundance in the natural world. It may be the bulk abundance in solar system matter. It may be the abundance outside a supernova that has just created new nuclei. It may be an isotopic anomaly within presolar grains having isotopic composition distinct from solar isotopes. It could be abundances within cosmic rays. Other examples exist. The point is that the observable should on good independent grounds be believed to measure the process modeled. Combination of 1 and 2 focuses on the cross section dependence of the value of an observable as produced in the process 1. It is then a separate question as to whether that cross section has a different importance for another observable, or within a different process. Such distinctions are necessary and valid.

The greater the sensitivity of the observable to the value of a specific reaction rate, the more important that rate’s value is. Not every abundance observable depends sensitively on the nuclear reaction rates; for such cases a cross section does not carry significance (for that observable and that process). When experiments are difficult and costly it would be discouraging to learn afterwards that the effort was without astrophysical significance. Our approach is to explicitly vary the reaction rate to measure the dependence of the final abundance of the observable to the value of that rate. By that procedure a quantitative measure of its significance can be presented.

Item 4, the strategy for the measurement, will be the issue decided by experimental teams motivated to nuclear research for purposes of nuclear astrophysics.

3. The ^{44}Ti Abundance in the Alpha-Rich Freezeout

The sensitivity of ^{44}Ti synthesis to variations in unmeasured cross sections must be determined for the process that produces it. Point 1 of §2.2 requires an appropriate model for that process, which is now known to be the alpha-rich freezeout of matter that was initially in nuclear statistical equilibrium or quasi-statistical equilibrium but that freezes out with excess alpha particles (Woosley et al. 1973; Thielemann, Hashimoto, & Nomoto 1990; Thielemann, Nomoto, & Hashimoto 1996). Although ^{44}Ti is also produced during silicon burning (Bodansky et al. 1968) and within explosive helium burning as it may occur within He caps atop Type Ia supernovae (Livne & Arnett 1995; Woosley, Taam, & Weaver 1986), it is believed that the alpha-rich freezeout

is responsible for most of natural ^{44}Ca and it is certain that it is responsible for the ^{44}Ti gamma lines detectable from young Type II remnants. We therefore choose in this work to determine the sensitivity of the ^{44}Ti yield within that process. It still remains to select an appropriate model for that process. Actual supernova models are both uncertain and complicated. In figure 1 we show contours of ^{44}Ti yields computed with our network code (described in more detail below) as functions of initial peak temperature and density in nearly adiabatically expanding matter experiencing an alpha-rich freezeout. The figure shows that the ^{44}Ti yield variation is less than a factor of 10 for quite large ranges of peak temperatures and densities near the reference parameters, which have been suggested by hydrodynamic models. Therefore, to survey the nuclear reaction rate sensitivity it will suffice to evaluate that rate sensitivity within parameterized expansions that are typical of the alpha-rich freezeout history within the Type II core. We do this by adiabatic expansions of pure ^{28}Si matter initially at $T_9 = T/10^9 \text{ K} = 5.5$ and mass density $\rho = 10^7 \text{ g cm}^{-3}$. These are the same conditions studied by Woosley & Hoffman (1991) for the alpha-rich freezeout (see their Table 1). Such conditions imply a ratio of the number density of photons to that of nucleons of 0.57, corresponding to a specific entropy $s/k \approx 5$, which is suitable for shock decomposed silicon in the Type II ejecta. We take the initial density to decline exponentially with an e-fold time 0.14 s, a typical hydrodynamical timescale, and we assume that the photon-to-nucleon ratio stays fixed at 0.57 throughout the expansion; thus, $\rho \propto T^3$. This one zone calculation is then allowed to cool until charged particle reactions freeze out ($T_9 \sim 0.25$). Such a schematic calculation, though inadequate to define the actual ^{44}Ti yield from core collapse supernovae, is adequate as the basis for a survey of cross-section sensitivity for that yield.

One additional parameter set by the presupernova evolution is the fractional neutron excess η of the matter undergoing the alpha-rich freezeout. Roughly speaking its value, which depends upon how far thermonuclear evolution has progressed when the shock wave strikes, is $\eta \simeq 0$ in the He core, $\eta \simeq 0.002$ (Z_i/Z_\odot) in the CO core, and $\eta \simeq 0.006$ in the Si core. We first survey at $\eta=0$ in section 4.

The reaction network used for the calculations is that described in Meyer (1995) and Meyer, Krishnan, & Clayton (1996). Table 1 shows the nuclides included in the network. Within explosive silicon burning that network includes many experimentally unknown reaction cross sections. For these reactions, the rates are calculated from the SMOKER code (Thielemann, Arnould, & Truran 1987).

Figure 2 shows the evolution of mass fractions of key species in the “standard” calculation. The material begins as pure ^{28}Si , but quickly breaks down into light particles which then establish a large quasi-equilibrium (QSE) cluster ranging from silicon to beyond nickel. For these particular conditions, the system does not attain complete nuclear statistical equilibrium (NSE). This is due to the slowness of the triple- α reaction in maintaining the abundance (per nucleon) Y_h of heavy nuclei ($A \geq 12$) at the level demanded by NSE. This slowness imposes an extra constraint on the equilibrium, which is thus a QSE, not an NSE (Meyer, Krishnan, & Clayton 1997). Within the QSE cluster the rates of reactions involving p , n , α , and γ reactions proceed at the same rate

as their inverses, just as in NSE; but in QSE the total number of nuclei in the cluster is not the number they would have in NSE.

As the temperature falls, the ^{44}Ti abundance drops. This is a consequence of the fact that the QSE cluster shifts upward in mass owing to falling temperature in the face of a deficit of heavy nuclei relative to NSE demands (Meyer, Krishnan, & Clayton 1996). ^{44}Ti breaks out of the large QSE cluster around $T_9 = 4.3$, and its abundance starts to grow as alpha particles in this alpha-rich freezeout reassemble into ^{12}C . Subsequent alpha captures then carry the newly assembled ^{12}C up to higher-mass nuclei, including ^{44}Ti . The final frozen ^{44}Ti mass fraction ends up roughly three orders of magnitude greater than its lowest value at the moment it broke out of the large QSE cluster. MPEG movies illustrating the nuclear dynamics of the “standard” calculation are available for viewing on the world-wide web at <http://photon.phys.clemson.edu/movies.html>

4. The Reaction-Rate Survey at $\eta=0$

In order to determine the sensitivity of the ^{44}Ti yield to specific reaction rates, we carried out a systematic survey. The central plan of the survey is to increase or decrease a reaction rate or set of reaction rates by a large factor and then to rerun the alpha-rich freezeout calculation described above. The associated errors in the nuclear cross sections may be either a uniform increase or decrease of their values as a function of energy within the statistical model, or they may be specific energy-dependent contributions to the reaction rate. We then compared the resulting ^{44}Ti yield to that in the “standard” calculation in which no reaction rate was changed. A significant yield difference indicates a sensitivity to the varied rates. It is important to note that the network code automatically computes reverse reaction rates from the (largely known) nuclear masses, forward reaction rates, and detailed balance; thus, for example, if the rate for the reaction $^{48}\text{Cr}(\alpha, \gamma)^{52}\text{Fe}$ is increased by a factor of 100, the code automatically increased the rate for the reverse reaction $^{52}\text{Fe}(\gamma, \alpha)^{48}\text{Cr}$ by a factor of 100. This is in compliance with detailed balance and is necessary to allow the network to relax to the appropriate equilibrium when relevant.

We began with a survey over element number Z . This step multiplies all charge-increasing and mass-increasing reaction rates on all isotopes of a single element Z by a factor of 0.01 and ran the alpha-rich freezeout. This set of reaction consists of (α, γ) , (α, p) , (α, n) , (p, γ) , (p, n) , (n, γ) . Elements from carbon ($Z = 6$) to bromine ($Z = 35$) are tested in this way. We then repeated the procedure, but this time using a factor of 100. The results are shown in figure 3. From this figure it is evident that the ^{44}Ti yield is sensitive to reaction rates on a number of elements, particularly on Ti itself and on V. What is perhaps more striking, however, especially in the lower panel, is the large number of elements to which the ^{44}Ti yield is *not* sensitive. For example, the ^{44}Ti yield (the astrophysically relevant observable) is not sensitive to large (factor of 100) uncertainties in reactions on any isotope of carbon through phosphorus! Such a negative result insofar as rate sensitivity is concerned is as valuable as a positive result because it increases the robustness of calculations of nucleosynthesis in alpha-rich freezeouts. The uncertainties in these cross sections

do not jeopardize the calculated ^{44}Ti yields. Understanding this prevents incorrect astrophysical motivations for nuclear experiments on reactions irrelevant to the observable.

There is a simple reason for the insensitivity of the ^{44}Ti yield to reaction-rate variations on so many elements. As discussed in the previous section, the ^{44}Ti abundance builds up as new heavy nuclei assemble late in the expansion. A nearly steady nuclear flow, whose magnitude is governed by the triple- α rate, carries these new nuclei up to higher mass. By steady flow, we mean that the nuclear flow into a nuclear species by capture from lower-mass nuclei equals the capture flow out of that species; thus, the abundance of the nuclear species in question does not change except over long time. Because the flow is given by a rate times an abundance, an increase in the rate is compensated by a decrease in the abundance so that the net nuclear flow upward remains unchanged. By analogy, if a smoothly flowing river widens at some point, its depth or its speed decreases in order to keep the same number of gallons per second moving downstream. As a particular nuclear example, a factor of 100 decrease in the ^{36}Ar abundance compensates the factor of 100 increase in the $^{36}\text{Ar}(\alpha, \gamma)^{40}\text{Ca}$ reaction rate in a steady flow. A large uncertainty in the $^{36}\text{Ar}(\alpha, \gamma)^{40}\text{Ca}$ rate would thus certainly be important for the yield of ^{36}Ar , but it is essentially irrelevant for our chosen observable, the ^{44}Ti yield. These considerations illustrate the importance of clearly defining the observable when discussing the importance of particular nuclear reactions.

Table 2 ranks by element the ^{44}Ti yield variation resulting from the survey over each element. The percent change is the increase in ^{44}Ti yield divided by the reference value, in parts per hundred. A large variation for a given element means that the final ^{44}Ti yield is sensitive to at least one reaction rate on some isotope of that element. The next task is to identify the key isotope. For each element showing a large ^{44}Ti -yield variation, we performed an isotope search by multiplying all reactions on a given isotope of that element Z by a factor of 0.01 and rerunning the alpha-rich freezeout. This was repeated for each isotope of the element Z in the network. After completing the isotope survey for element Z , we surveyed the next important element. This entire procedure was then repeated but with a factor 100 multiplying the reaction rates.

Figure 4 shows the results for the isotope surveys for Ar, Ca, Ti, and V for both the 0.01 and 100 factors. It demonstrates that the ^{44}Ti yield significantly varies for changes on only one isotope of each of the elements. For the elements shown, these are ^{36}Ar , ^{40}Ca , ^{44}Ti , and ^{45}V . Table 3 ranks the particular isotopes for the 0.01 and 100 reaction-rate variation surveys. Comparing the first entries of tables 2 and 3, for example, shows that a 100-fold decrease of the reaction rates for all Ti isotopes produces an almost identical increase (+373%) in final ^{44}Ti abundance, in comparison to the increase (+372%) for the ^{44}Ti reaction rate only.

With the key isotopes now identified, we next determined which particular nuclear reaction dominated the sensitivity of the ^{44}Ti yield. This step of the survey, similar to that done above, varied a specific reaction on the key isotope. The first such survey was of the nuclear reactions on ^{45}V . We multiplied the $^{45}\text{V}(n, \gamma)^{46}\text{V}$ rate by a factor of 0.01 and reran the alpha-rich freezeout. We then repeated this for the (p, γ) , (p, n) , (α, γ) , (α, n) , and (α, p) reactions. We did this for

each isotope listed in table 3. We then repeated the procedure with a multiplication factor 100.

The results for the surveys on ^{40}Ca , ^{44}Ti , ^{45}Ti , and ^{54}Fe are shown in figure 5. Its discrete abscissa is the reaction channel for that isotope. The results clearly show that the ^{44}Ti yield is sensitive to variations in the rates of the particular reactions $^{40}\text{Ca}(\alpha, \gamma)^{44}\text{Ti}$, $^{44}\text{Ti}(\alpha, p)^{47}\text{V}$, $^{44}\text{Ti}(\alpha, \gamma)^{48}\text{Cr}$, $^{45}\text{V}(p, \gamma)^{46}\text{Cr}$, and $^{54}\text{Fe}(\alpha, n)^{57}\text{Ni}$. Table 4 ranks the particular nuclear reactions according to their influence at $\eta=0$ on the final ^{44}Ti yield. For example, reduction of $^{44}\text{Ti}(\alpha, \gamma)^{48}\text{Cr}$ has almost no effect (unless of course the (α, p) branch is also reduced), whereas increase of its rate by $100\times$ is almost as effective as an increase of the (α, p) channel. Such conclusions depend on the relative magnitude of proton and gamma widths of the compound nuclear states, and on the factor by which they are altered. Owing to its special role in the late assembly of heavy nuclei, we also surveyed the triple- α reaction and include it in table 4.

One might have predicted that a number of these reactions would be important, although the magnitude of their effects would not have been as easy to guess. The $^{45}\text{V}(p, \gamma)^{46}\text{Cr}$ reaction, the one showing the largest effect, however, was not one for which we had anticipated a special role. This underscores the importance of making a systematic survey when considering the reaction-rate sensitivity of a particular observable. In fact, not only are systematic surveys important for clearly delineating reaction-rate sensitivities, but they can also clarify nucleosynthesis. It was only after developing new insights into the nuclear dynamics of an alpha-rich freezeout that we were able to understand the reason for the importance of the $^{45}\text{V}(p, \gamma)^{46}\text{Cr}$ reaction. By the same token we can understand why its importance vanishes for neutron richness $\eta > 0.0004$ (see Section 6). We return to this issue in the next section.

The remaining task for the ^{44}Ti survey was to determine the form of the sensitivity of each particular important reaction. Figure 5 shows that increasing the $^{45}\text{V}(p, \gamma)^{46}\text{Cr}$ reaction by a factor of 100 decreases the resulting ^{44}Ti yield by a factor of nearly 50. This suggests a nearly linear dependence of the ^{44}Ti yield on the rate of this reaction. For a decrease by a factor of 100 on this rate, however, the ^{44}Ti yield increases by less than a factor of two, suggesting a non-linear dependence. The yield dependence on the rate value determines its significance. To quantify the form of the dependence, the alpha-rich freezeout was repeated many times, each time with a specific important nuclear reaction rate multiplied by a factor between 0.01 and 100. This maps out the sensitivity of the ^{44}Ti yield to any change by a factor between 0.01 and 100 on the important nuclear reactions. Figures 6, 7, 8, and 9 show results of such surveys. In each of these figures, a small solid square indicates the result using the “standard” value for that particular rate.

These figures illuminate more subtle aspects of the reaction rate sensitivities. Figure 6 shows that a factor of two increase or decrease in the $^{45}\text{V}(p, \gamma)^{46}\text{Cr}$ rate results in a $\sim 20\%$ change in the yield of ^{44}Ti . On the other hand, figure 8 shows that a factor of two change in the $^{44}\text{Ti}(\alpha, \gamma)$ reaction rate barely changes the ^{44}Ti yield, even though a factor of 100 increase in the rate dramatically drops the yield. Because the reaction rates we use are either experimentally known or among the best theoretical estimates presently available, we expect the true rates in general

not to be more than, say, an order of magnitude different. Thus, the quantity expressing the ^{44}Ti -sensitivity to a particular reaction near its reference value is the slope of the curve for that reaction, in analogy to figure 6. In table 5 we present these quantities, in a ranking by magnitude, for the sixteen most important reactions at $\eta=0$ insofar as final ^{44}Ti abundance is concerned.

As an example of how to use table 5, consider the case of $^{45}\text{V}(p, \gamma)^{46}\text{Cr}$. If it were measured, one would then compare that rate (especially near $T_9 = 2$ for reasons to be discussed in the next section) to the value used in our surveys, the fits for which we present in table 8. If the measured rate were a factor of 1.5 greater than the tabulated value for all temperatures, the resulting ^{44}Ti yield would change by $-0.361 \times (1.5 - 1) = -0.18 = -18\%$, that is, it would be 82% of the standard value.

It was only through a large and systematic survey that we were able to determine the relative importance of the reactions listed in table 5. This was a computationally intensive effort comprising more than 2000 sets of alpha-rich freezeout calculations, each taking ~ 20 minutes on a 200 MHz DEC Alpha workstation. Nevertheless, it is only in this way that one can be fully confident of understanding the reaction-rate sensitivity of the ^{44}Ti yield.

A final part of the survey applies to neutron-excess η greater than zero. The survey is repeated in summary form in Section 6 for $\eta = 0.002$ and $\eta = 0.006$. For these neutron enrichments, ^{44}Ti synthesis was unaffected by the value of the $^{45}\text{V}(p, \gamma)^{46}\text{Cr}$ reaction rate, a result also explained in Section 6. But first we describe the reasons for the importance of the Table 4 reactions at $\eta = 0$.

5. Discussion of the Most Important Reactions

Table 5 lists the reactions to which the ^{44}Ti yield is most sensitive in an alpha-rich freezeout. In this section, we briefly explore the reasons for this sensitivity for three important reactions. In addition to the immediate interest of understanding the importance of these reactions, this exercise provides new insights into the nuclear dynamics of the alpha-rich freezeout.

Any nucleosynthetic system seeks to maximize its entropy and thereby to achieve an equilibrium. Its ability to do this, however, is governed by the rate of certain key reactions. When a particular reaction becomes too slow, the equilibrium breaks. The system still maximizes the entropy, but the slowness of the particular reaction adds a constraint which restricts the number of accessible states (Meyer, Krishnan, & Clayton 1997). As the system evolves toward lower temperatures, more reactions become slow, more equilibria break, and more constraints are added to the entropy maximum. In this way, the system descends the “hierarchy of statistical equilibria” (contribution of Meyer in Wallerstein et al. 1997). Several of the reactions in table 5 are important because they control the breaking of equilibria and, thus, the descent of the hierarchy. Other reactions are important because they control when the steady (but non-equilibrium) flow into ^{44}Ti breaks down or because they control the economy of light particles that influence the abundance of ^{44}Ti late in the expansion.

5.1. The triple- α reaction

We begin with the triple- α reaction. Figure 10 shows the time history of the ^{44}Ti mass fraction during two alpha-rich freezeouts—one with the standard (Caughlan & Fowler 1988) rate (dashed curve) and one with the standard rate increased by a factor of 100 (solid curve). For comparison, the dotted curve gives the ^{44}Ti mass fraction in NSE. This NSE is calculated at each timestep in the expansion using the same temperature, density, and neutron richness as in the network. The dashed and solid curves differ throughout the expansions. In the case with the increased triple- α rate, the nuclear system achieves and maintains NSE for the early part of the expansion. With the standard triple- α rate, the system never reaches NSE but rather only a QSE in which the number of heavy nuclei Y_h differs from that in NSE. Below $T_9 \approx 5.3$ the number of heavy nuclei in the standard run QSE is less than that in NSE, so the heavy nuclei are in the presence of an overabundance (relative to NSE) of light particles. This favors nuclei heavier than ^{44}Ti (e.g. ^{56}Ni), so the ^{44}Ti mass fraction is far below that of NSE until later in the expansion when the large QSE breaks and the ^{44}Ti can build back up without being driven upward to ^{56}Ni .

The ^{44}Ti mass fraction in the standard calculation is less than that in the case with the increased triple- α reaction for $T_9 < 5.3$. The latter expansion deviates from NSE beginning at $T_9 \approx 5.2$. At this point the nuclear system is also in a QSE, but this QSE has a greater number of heavy nuclei and a smaller number of light particles than the standard case QSE. This yields a greater mass fraction of ^{44}Ti within the QSE cluster. At the point ^{44}Ti breaks out of the large QSE cluster containing ^{56}Ni (the dip in both curves near $T_9 = 4$), the ^{44}Ti mass fraction in the expansion with the increased triple- α rate exceeds that in the standard case by a factor of \sim eight. More importantly, the expansion with the increased triple- α rate has a factor of ~ 4.6 lower mass fraction of ^4He . Remarkably, this factor of 4.6 (when cubed) compensates for the increased triple- α cross section; thus, the two expansions create new nuclei at the nearly the same rate at late times. The crucial aspect for ^{44}Ti is that the lower ^4He abundance in the expansion with the increased triple- α cross section requires larger abundances of nuclei between ^{12}C and ^{56}Ni to carry the same flow. This causes the increase in the final yield of ^{44}Ti .

5.2. $^{44}\text{Ti}(\alpha, p)^{47}\text{V}$

Figure 11 shows the ^{44}Ti mass fraction in the standard calculation (dashed curve) and in an expansion with the $^{44}\text{Ti}(\alpha, p)^{47}\text{V}$ rate increased by a factor of 100. Also shown as the dotted curve is the QSE mass fraction of ^{44}Ti in the standard expansion calculated at each timestep from the same temperature, density, neutron richness, and number of heavy nuclei as in the network. The evolution of the ^{44}Ti mass fraction follows QSE in both cases down to $T_9 \approx 4.5$. The increased $^{44}\text{Ti}(\alpha, p)^{47}\text{V}$ rate, however, allows the ^{44}Ti to remain in QSE with ^{56}Ni longer; thus, when the QSE finally breaks, the ^{44}Ti mass fraction is ~ 30 times lower than the corresponding value in the standard case. This result illustrates the important role $^{44}\text{Ti}(\alpha, p)^{47}\text{V}$ plays in linking the Si-Ca

QSE cluster to the Ni-centered QSE cluster (Woosley et al. 1973; Hix & Thielemann 1996). Once the two clusters fall out of equilibrium with each other, the $^{44}\text{Ti}(\alpha, p)^{47}\text{V}$ reaction governs the rate at which abundance moves from the Si-Ca-Ti cluster to the Ni cluster. A faster rate gives a lower abundance in the Si-Ca-Ti cluster and a lower ^{44}Ti yield.

5.3. $^{45}\text{V}(p, \gamma)^{46}\text{Cr}$

Perhaps the biggest surprise in our survey was the importance of the $^{45}\text{V}(p, \gamma)^{46}\text{Cr}$ reaction. Figure 12 shows the ^{44}Ti mass fraction for the standard calculation (dashed curve) and for an expansion with the $^{45}\text{V}(p, \gamma)^{46}\text{Cr}$ increased by a factor of 100. The ^{44}Ti evolution is precisely the same in the two expansions down to $T_9 \approx 2$. The subsequent deviation between the two cases, however, is dramatic. While the ^{44}Ti mass fraction drops by $\sim 30\%$ as T_9 falls below 2 in the standard calculation, it plummets by a factor of ~ 100 for the increased $^{45}\text{V}(p, \gamma)^{46}\text{Cr}$ rate. The reason is, as in the previous cases, that this reaction controls the breaking of an equilibrium.

The equilibrium of importance in this case is a $(p, \gamma) - (\gamma, p)$ equilibrium among the $N = 22$ isotones. In such equilibrium, the rates (as opposed to the cross sections) of (p, γ) reactions proceed at the same rates as the reverse (γ, p) reactions; i.e. $^A\text{Z} + p \rightleftharpoons ^{A+1}(\text{Z}+1) + \gamma$, where the reversed arrows indicate equal numbers of reactions per unit time. We focus on the $N = 22$ isotones, $A = Z + 22$. Figure 13 shows how this equilibrium breaks for the standard set of cross sections. It gives for four temperatures the ratio of the network abundance of these isotones to the values they would have in $(p, \gamma) - (\gamma, p)$ equilibrium. For $T_9 = 2.66$, all of the isotones for Ti through Fe are in equilibrium with each other under exchange of protons, but the lower-charge isotones have already broken out of this equilibrium. As the temperature falls to $T_9 = 2.15$, ^{48}Fe strongly falls out of equilibrium with the other four species, but also evident is the fact that the two small equilibrium clusters (^{44}Ti & ^{45}V) and (^{46}Cr & ^{47}Mn) are starting to fall out of equilibrium with each other; that is, ^{45}V and ^{46}Cr are no longer in $(p, \gamma) - (\gamma, p)$ equilibrium with each other. This break grows with decreasing temperature. By $T_9 = 1.81$ the two small $(p, \gamma) - (\gamma, p)$ clusters, (^{44}Ti & ^{45}V) and (^{46}Cr & ^{47}Mn), are strongly out of equilibrium with each other. When this occurs, $^{45}\text{V}(p, \gamma)^{46}\text{Cr}$ produces net destruction of ^{45}V , and hence of ^{44}Ti , with which it is in equilibrium.

The $T_9 = 1.81$ panel of this figure shows that the $^{44}\text{Ti}-^{45}\text{V}$ cluster is overabundant and the $^{46}\text{Cr}-^{47}\text{Mn}$ cluster is underabundant with respect to the overall $(p, \gamma) - (\gamma, p)$ equilibrium. This indicates that too few nuclei have moved from the $^{44}\text{Ti}-^{45}\text{V}$ cluster up to the $^{46}\text{Cr}-^{47}\text{Mn}$ cluster because of the slowness of the reaction that links them, namely, $^{45}\text{V}(p, \gamma)^{46}\text{Cr}$. By increasing the rate of this reaction, the two small clusters remain in equilibrium with each other longer, the $N = 22$ isotones shift to higher mass, and more ^{44}Ti is destroyed.

The dotted curve in figure 12 amplifies this point by showing what would happen in the standard case to the ^{44}Ti mass fraction if the $(p, \gamma) - (\gamma, p)$ equilibrium among $N = 22$ isotones persisted to low temperature. The faster $^{45}\text{V}(p, \gamma)^{46}\text{Cr}$ reaction allows the ^{44}Ti to remain in the

$(p, \gamma) - (\gamma, p)$ equilibrium to lower temperature. Because the $(p, \gamma) - (\gamma, p)$ equilibrium abundances shift to higher mass with lower temperature, the ^{44}Ti mass fraction falls. Even with the fast $^{45}\text{V}(p, \gamma)^{46}\text{Cr}$ reaction, however, the equilibrium eventually breaks and the ^{44}Ti mass fraction freezes out. In the surveys at greater neutron excess to follow, we demonstrate that the controlling significance of $^{45}\text{V}(p, \gamma)^{46}\text{Cr}$ vanishes for $\eta > 0.0004$. This will be understood as a consequence of the smaller free proton density with increased η .

6. Surveys Having Excess Neutrons

We repeated the surveys in exactly the same procedure for a nuclear gas containing more neutrons than protons in total. This initial neutron richness, when the shock wave strikes the overlying matter, is not altered during the subsequent rapid nuclear burning, which occurs too rapidly for significant electron capture to occur. Thus the gas can be described by a constant parameter $\eta = \sum_i (N_i - Z_i)Y_i$, where N_i and Z_i are the mass fractions of nucleons (both bound in species i and free) and $Y_i \equiv X_i/A_i$ is the abundance of species i with mass fractions X_i and atomic mass number A_i . The survey shows that although most nuclear reactions retain their importance for ^{44}Ti production during alpha-rich freezeouts, the $^{45}\text{V}(p, \gamma)^{46}\text{Cr}$ reaction is very sensitive to the value of η . Demonstrating and understanding these facts is the main goal of this section.

The range of anticipated values for η is set by the presupernova evolution and structure and by the strength of the shock wave. The latter determines how far radially the shock can propagate with sufficient strength to establish an alpha-rich freezeout, without which the yield of ^{44}Ti is too small to contribute substantially to the natural ^{44}Ca abundance. Within the entire He core of massive stars the matter is dominated by He, ^{14}N , ^{16}O and ^{12}C , all of which have $\eta = 0$. But within the CO core η has been increased by the conversion of ^{14}N to ^{18}O and ^{22}Ne , both of which have two excess neutrons. At solar initial metallicity (Z_\odot) these comprise about 2% by mass, so that $\eta = 0.002$ throughout the CO core. Supernovae of lower initial metallicity Z_i , such as supernova 1987A in the Magellanic Cloud, will have η near $0.002(Z_i/Z_\odot)$ in their CO cores. Hydrostatic carbon burning does not much increase η within the NeMg core, but hydrostatic O burning does do so. The more central core in which O has burned to create a Si core has acquired more excess neutrons by electron captures on the products of O burning (Woosley, Arnett, & Clayton 1972), yielding η in the range 0.003-0.006. In the interests of limiting the computational demands, we have performed the full survey at the values $\eta = 0.002$ and 0.006 . Finer precision mapping in η was also done for the $^{45}\text{V}(p, \gamma)^{46}\text{Cr}$ reaction alone, after determining its sensitivity to the neutron excess.

Tables 6 and 7 list the effect of reaction rate changes for the ten most important regulators of ^{44}Ti production at these two values of η . Many of the same reactions remain important, such as $^{44}\text{Ti}(\alpha, p)^{47}\text{V}$, $^{40}\text{Ca}(\alpha, \gamma)^{44}\text{Ti}$, and $^{36}\text{Ar}(\alpha, p)^{39}\text{K}$; but the importance of $^{45}\text{V}(p, \gamma)^{46}\text{Cr}$ disappears and some new important reactions appear (e.g. $^{12}\text{C}(\alpha, \gamma)^{16}\text{O}$). More complete lists can be read and downloaded from the Clemson nuclear astrophysics web site

(<http://photon.phys.clemson.edu/tables.html>).

In the interest of understanding we comment upon two of these dramatic changes. The importance of the $^{45}\text{V}(\text{p},\gamma)^{46}\text{Cr}$ reaction declines precipitously for $\eta > 0.0001$, as shown in figure 14. The cause is the decline of the free-proton abundance Y_p at every temperature with increasing η . As η increases, protons tend to be more tightly bound in nuclei. Although the $^{44}\text{Ti}-^{45}\text{V}$ pair remain in (p,γ) equilibrium down to $T_9 \lesssim 2$ for η as large as ~ 0.01 , the ^{45}V abundance is declining with increasing η due to the diminishing free proton abundance. As a result the final proton captures are unable to reduce the abundance of the $^{44}\text{Ti}-^{45}\text{V}$ pair during the freezeout. Figure 14 shows the free proton abundance at $T_9 = 2$, the temperature at which the (p,γ) equilibrium begins its freezeout, for several calculations at different η 's. In the equilibrium, the abundance ratio $^{45}\text{V}/^{44}\text{Ti} \propto Y_p$. The $^{45}\text{V}(\text{p},\gamma)^{46}\text{Cr}$ reaction rate is also proportional to Y_p ; thus, the importance of this reaction rate in modifying the final ^{44}Ti yield goes as Y_p^2 . The fact that Y_p at $T_9 = 2$ drops off so rapidly for $\eta > 0.0001$ explains why the final ^{44}Ti yield sensitivity also declines so quickly. The consequence is that the $^{45}\text{V}(\text{p},\gamma)^{46}\text{Cr}$ reaction loses considerable importance for observations of ^{44}Ti in supernovae, at least unless they have very small initial metallicity, or unless the shock wave is able to reach the He shell, or unless some other process keeps the proton abundance higher than would be expected simply from the alpha-rich freezeout. It is worth noting that some Type Ia events create abundant ^{44}Ti (Clayton et al. 1997); but the burning is not literally an alpha-rich freezeout although it does have hot excess alpha particles. A variety of η 's might be expected in this scenario depending on the initial composition. For low η we will again expect certain proton capture reactions to affect the ^{44}Ti yield. We will study the important cross sections for many observables in this setting in a subsequent work in this series.

The $^{12}\text{C}(\alpha,\gamma)^{16}\text{O}$ reaction assumes greater importance for $\eta > 0$. The greater neutron richness of the matter causes alpha particles to bind more tightly into nuclei, thereby decreasing the alpha particle abundance throughout most of the expansion. Because of the smaller alpha particle abundance, flow of newly assembled nuclei to higher mass freezes out at higher temperature. When the cross section for alpha particle capture on ^{12}C is decreased, this freezeout occurs even earlier, leading to considerably reduced ^{44}Ti production.

7. Conclusion

We have analyzed the influence of individual reaction rates on ^{44}Ti production in alpha-rich freezeouts within Type II supernova events. Using direct surveys we have established that the ^{44}Ti production at $\eta = 0$ is most sensitive to the following reaction rates: $^{45}\text{V}(\text{p},\gamma)^{46}\text{Cr}$, $\alpha(2\alpha,\gamma)^{12}\text{C}$, $^{44}\text{Ti}(\alpha,\text{p})^{47}\text{V}$, $^{44}\text{Ti}(\alpha,\gamma)^{48}\text{Cr}$, $^{40}\text{Ca}(\alpha,\gamma)^{44}\text{Ti}$, and $^{57}\text{Co}(\text{p},\text{n})^{57}\text{Ni}$. For $\eta > 0$ the two proton-induced reactions decline rapidly in importance and some other reactions become crucial: $^{12}\text{C}(\alpha,\gamma)^{16}\text{O}$, $^{40}\text{Ca}(\alpha,\gamma)^{44}\text{Ti}$, $^{27}\text{Al}(\alpha,\text{n})^{30}\text{P}$, and $^{30}\text{Si}(\alpha,\text{n})^{33}\text{S}$. Several good reasons justify this effort at a depth of detail and computational time that exceeds that normally devoted to nuclear studies in astrophysics. Three main reasons are: (1) to provide guidelines for laboratory measurements;

(2) to establish better diagnostics of supernova events; (3) to gain insight into complicated and nonlinear nuclear reaction networks of importance for nucleosynthesis.

The first reason parallels the large increase in recent activity in laboratory nuclear astrophysics. In particular, many new radioactive-ion-beam facilities are rapidly establishing the capability to measure reaction cross sections near and on the proton-rich side of the $Z = N$ line. This capability opens to experimental study nucleosynthesis processes that have heretofore had to rely on computed cross sections. Each such experiment will be costly and time consuming, however, so that solid grounds for the importance of any specific reaction are welcome to experimental planners.

The second reason parallels the large increase in recent observations of supernova nucleosynthesis. Although the mass of ^{44}Ti within the Cas A supernova 310-year-old remnant cannot yet be regarded as measured with good precision, the recent detection of it insures that it eventually will be well measured. When that precision has been achieved, the mass of ^{44}Ti will reflect the alpha-rich-freezeout mass that was ejected. Since this mass depends in exciting ways on the physics that underlies the Type II event (the mass cut and the shock mechanism), all manner of exciting issues may hinge upon its production. The same will be true for the several recent Galactic supernovae that will be detected with the improved gamma-ray detector sensitivity that now exists in laboratories. It is probable that significant variations of the ^{44}Ti yield exist between different events. Once that observational goal is achieved, the most accurate cross sections will be wanted so that the scientific uncertainties reflect the uncertainties over the realistic supernova model rather than over the nuclear cross sections. Similar excitement attends the measurement of $^{44}\text{Ti}/^{48}\text{Ti}$ production ratios in samples of supernova matter as recorded by supernova condensates found in meteorites. One does not want nuclear cross section uncertainties to stand in the way of quantitative analysis.

The third reason parallels the large recent increase in the sophistication with which nucleosynthesis is viewed. The present study illuminates this very well. Within the complex networks of explosive nucleosynthesis, one can ideally think of the importance of any specific nuclear reaction in various ways. It may have almost no significance if that reaction maintains a partial QSE throughout the burning. When QSE breaks down or fragments, a reaction may play a rather complicated role in governing the changing relative total numbers within the different QSE clusters; or it may play a role in the density of free light particles; or it may simply be the specific channel by which an abundance is altered in the freezeout. The important reactions identified by us for ^{44}Ti production in the alpha-rich freezeout reveal each of these aspects. We have discussed these to some extent in the discussions of the important reactions.

Finally we would observe that our study concentrated on one very important nucleus within one nucleosynthesis process. There are many nucleosynthesis processes producing many different nuclei, so additional studies of the present type are recommended. This requires judgment as well as computing power. Clearly one does not wish to have huge numbers of irrelevant studies

performed. For this reason, such studies should follow the “four-requirement” structure outlined in §2.2.

We would like to thank the referee, Robert Hoffman for a thorough review and suggestions to improve this paper. This work has been supported by NASA grants NAG5-4329 and NAGW-3277.

REFERENCES

Alburger, D. E., and Harbottle, G. 1990, Phys. Rev. C, 41, 2320

Amari, S., Hoppe, P., Zinner, E., & Lewis, R. S. 1992, ApJ, 394, L43

Ashworth, W.B. 1980, J. History Astron., 11, 1

Bodansky, D., Clayton, D. D., & Fowler, W. A. 1968, ApJS, 16, 299

Caughlan, G. R., & Fowler, W. A. 1988, At. Data Nucl. Data Tables, 40 283

Clayton, D. D. 1971, Nature, 234, 291

Clayton, D. D. 1975, Nature, 257, 36

Clayton, D. D., Arnett, D., Kane, J., & Meyer, B. S. 1997, ApJ, 486, 824

Clayton, D. D., Amari, S., & Zinner, E. 1997, Ap&SS, 251, 355

Dupraz, C., Bloemen, H., Bennett, K., Diehl, R., Hermsen, W., Iyudin, A. F., Ryan, J., and Schönfelder, V. 1997, A&A, 324, 683

Görres, J. et al. 1998, PRL, in press

Hartmann, D. et al. 1993, in Proc. of the Compton Observatory Science Workshop, eds. C. R. Shrader, N. Gehrels, & B. Dennis, NASA CP, No. 3137, (Greenbelt, Maryland: NASA), 388

Hix, W. R., & Thielemann, F.-K. 1996, ApJ, 460, 869

Hoppe, P., Strebler, R., Eberhardt, P., Amari, S. and Lewis, R. S. 1996, Science, 272, 1314

Iyudin, A. et al. 1994, A&A, 284, L1

Iyudin, A. et al. 1997, in Proc. of the 2nd. INTEGRAL Workshop, eds. C. Winkler, T.J.-L. Courroisier, Ph. Durouchoux, ESA Publications Div, 37

Jin, L., Meyer, B. S., The, L.-S., & Clayton, D. D. 1997, Nucl. Phys. A621, 391c

Leising, M. D., & Share, G. H. 1994, ApJ, 424, 200

Livne, E. & Arnett, W.D. 1995, *ApJ*, 452, 62

Lubkin, G. B. 1997, *Physics Today*, 50, 17

Mahoney, W. A., Ling, J.C., Wheaton, W. A., & Higdon, J.C. 1992, *ApJ*, 387, 314

Meissner, J. 1996, Ph.D. Thesis, Univ. of Notre Dame

Meyer, B. S. 1995, *ApJ*, 449, L55

Meyer, B. S., Krishnan, T. D., & Clayton, D. D. 1996, *ApJ*, 462, 825

Meyer, B. S., Krishnan, T. D., & Clayton, D. D. 1997, *ApJ*, in press

Nagataki, S., Hashimoto, M., Sato, K., & Yamada, S. 1997, *ApJ*, 486, 1026

Nittler, L. R., Amari, S., Zinner, E., Woosley, S. E., & Lewis, R. S. 1996, *ApJ*, 462, L31

Norman, E. B., et al. 1997, submitted to *Phys. Rev. C*

Rauscher, T., Thielemann, F.-K., & Kratz, K.-L. 1997, *Phys. Rev. C*, 56, 1613

Reed, J. E., Hester, J. J., Fabian, A. C., & Winkler, P. F. 1995, *ApJ*, 440, 706

Rothschild, R. E., et al. 1998, *Nucl. Phys. B*, submitted

The, L.-S., Leising, M. D., Clayton, D. D., Johnson, W. N., Kinzer, R. L., Kurfess, J. D., Strickman, M. S., Jung, G. V., Grabelsky, D. A., Purcell, W. R., and Ulmer, M. P. 1995, *ApJ*, 444, 244

The, L.-S., Leising, M. D., Kurfess, J. D., Johnson, W. N., Hartmann, D. H., Gehrels, N., Grove, J. E., and Purcell, W. R. 1996, *A&AS*, 120, 311

Thielemann, F.-K., Arnould, M., & Truran, J. W. 1987, in *Advances in Nuclear Astrophysics* eds. E. Vangioni-Flam, J. Audouze, M. Cassé, J.-P. Chièze, & J. Tran Thanh Van (Gif-sur-Yvette: Éditions Frontière), 525

Thielemann, F.-K., Hashimoto, M., and Nomoto, K. 1990, *ApJ*, 349, 222

Thielemann, F.-K., Nomoto, K., and Hashimoto, M. 1996, *ApJ*, 460, 408

Timmes, F. X., Woosley, S. E., Hartmann, D. H., and Hoffman, R. D. 1996, *ApJ*, 464, 332

Wallerstein, G. et al. 1997, *Rev. Mod. Phys.*, 69, 995

Woosley, S. E., Arnett, W. D., and Clayton, D. D. 1972, *ApJ*, 175, 131

Woosley, S. E., Arnett, W. D., and Clayton, D. D. 1973, *ApJS*, 26, 231

Woosley, S. E., and Hoffman, R. D. 1991, *ApJ*, 368, L31

Woosley, S. E. , Taam, R.E. & Weaver, T. A. 1986, ApJ, 301, 601

Table 1. Nuclei in the Network

Proton Number, Z	A_{min}	A_{max}
1	2	3
2	3	4
3	6	8
4	7	10
5	8	11
6	11	14
7	12	15
8	14	19
9	16	21
10	18	24
11	19	27
12	20	27
13	22	30
14	23	31
15	27	34
16	28	37
17	31	40
18	32	43
19	35	48
20	36	49
21	40	49
22	42	50
23	44	50
24	44	50
25	46	59
26	47	60
27	50	63
28	51	65
29	57	70
30	59	71
31	59	79
32	62	80
33	65	85
34	68	88
35	69	91

Table 2. Order of importance of elements affecting the ^{44}Ti production in alpha-rich freezeout mechanism if the nuclear cross sections for all mass or charge increasing reaction channels on all isotopes of an element are changed by a factor of 1/100 or 100.

Rank	Reaction rate			Reaction rate		
	multiplied by 1/100		multiplied by 100			
	Element	% ^{44}Ti change	Element	% ^{44}Ti change		
1	Ti	+372.6	V	-98.0		
2	Ca	-72.6	Ti	-91.3		
3	V	+56.6	Co	+30.6		
4	Ni	-52.3	Ca	+28.9		
5	Ar	-49.8	Fe	+9.2		
6	Co	-33.6	Ni	+7.1		
7	S	-20.8	Ar	+6.2		
8	Cu	-14.8	Cr	-5.9		
9	N	-14.8	Cu	+5.6		
10	Si	-4.5	Na	-2.4		
11	Ne	-4.0	Mn	+1.9		
12	C	+3.1	C	-1.8		
13	Cr	+2.9	N	-1.5		
14	Na	-1.7	Mg	+1.0		
15	K	-1.7	S	+0.8		
16	Al	+0.8	Zn	+0.5		
17	Fe	+0.7	Ne	+0.4		
18	Mg	-0.6	Al	-0.3		
19	Mn	-0.5	Si	+0.3		
20	Zn	-0.4	P	-0.2		
21	O	+0.4	Cl	+0.2		
22	P	+0.1	K	-0.1		
23	Sc	-0.1	Sc	+0.0		

Table 3. The Order of Importance of Isotope to the ^{44}Ti final mass fraction when all mass or charge increasing nuclear reactions of the isotope are multiplied by 1/100 or 100.

Rank	Reaction rate		Reaction rate	
	multiplied by 1/100	Isotope % ^{44}Ti change	multiplied by 100	Isotope % ^{44}Ti change
1	^{44}Ti	+371.7	^{45}V	-98.0
2	^{40}Ca	-72.5	^{44}Ti	-91.2
3	^{45}V	+56.6	^{57}Co	+27.1
4	^{36}Ar	-49.7	^{40}Ca	+22.0
5	^{57}Ni	-49.5	^{57}Ni	+11.5
6	^{57}Co	-33.0	^{54}Fe	+9.4
7	^{32}S	-20.4	^{36}Ar	+5.6
8	^{13}N	-14.8	^{46}Cr	-5.3
9	^{58}Cu	-13.5	^{56}Ni	-5.2
10	^{56}Ni	-4.5	^{61}Cu	+4.0
11	^{28}Si	-4.2	^{58}Ni	+3.4
12	^{56}Co	-4.1	^{23}Na	-2.6
13	^{20}Ne	-4.0	^{12}C	-1.8
14	^{12}C	+3.1	^{13}N	-1.5
15	^{48}Cr	+2.8	^{58}Cu	+1.3
16	^{39}K	-2.0	^{38}Ca	+1.0
17	^{14}O	+1.0	^{24}Mg	+0.9
18	^{27}Al	+0.9	^{59}Cu	+0.9
19	^{16}O	-0.8	^{32}S	+0.8
20	^{24}Mg	-0.6	^{48}Cr	-0.6

Table 4. Order of importance of reactions producing ^{44}Ti at $\eta=0$ from low multiplication factor ($0.01\times$) and high multiplication factor ($100\times$).

Rank	Reaction rate multiplied by 1/100		Reaction rate multiplied by 100	
	Reaction	% ^{44}Ti change	Reaction	% ^{44}Ti change
1	$^{44}\text{Ti}(\alpha, p)^{47}\text{V}$	+173	$^{45}\text{V}(p, \gamma)^{46}\text{Cr}$	-98
2	$\alpha(2\alpha, \gamma)^{12}\text{C}$	-100	$\alpha(2\alpha, \gamma)^{12}\text{C}$	+67
3	$^{40}\text{Ca}(\alpha, \gamma)^{44}\text{Ti}$	-72	$^{44}\text{Ti}(\alpha, p)^{47}\text{V}$	-89
4	$^{45}\text{V}(p, \gamma)^{46}\text{Cr}$	+57	$^{44}\text{Ti}(\alpha, \gamma)^{48}\text{Cr}$	-61
5	$^{57}\text{Ni}(p, \gamma)^{58}\text{Cu}$	-47	$^{57}\text{Co}(p, n)^{57}\text{Ni}$	+25
6	$^{57}\text{Co}(p, n)^{57}\text{Ni}$	-33	$^{40}\text{Ca}(\alpha, \gamma)^{44}\text{Ti}$	+22
7	$^{13}\text{N}(p, \gamma)^{14}\text{O}$	-16	$^{57}\text{Ni}(n, \gamma)^{58}\text{Ni}$	+10
8	$^{58}\text{Cu}(p, \gamma)^{59}\text{Zn}$	-14	$^{54}\text{Fe}(\alpha, n)^{57}\text{Ni}$	+9.4
9	$^{36}\text{Ar}(\alpha, p)^{39}\text{K}$	-11	$^{36}\text{Ar}(\alpha, p)^{39}\text{K}$	+5.5
10	$^{12}\text{C}(\alpha, \gamma)^{16}\text{O}$	+3.5	$^{36}\text{Ar}(\alpha, \gamma)^{40}\text{Ca}$	+5.3

Table 5. Order of Importance of Reactions Producing ^{44}Ti at $\eta = 0$ According to the Slope of $X(^{44}\text{Ti})$ Near the Standard Cross Section

Reaction	Slope
$^{44}\text{Ti}(\alpha, p)^{47}\text{V}$	-0.394
$\alpha(2\alpha, \gamma)^{12}\text{C}$	+0.386
$^{45}\text{V}(p, \gamma)^{46}\text{Cr}$	-0.361
$^{40}\text{Ca}(\alpha, \gamma)^{44}\text{Ti}$	+0.137
$^{57}\text{Co}(p, n)^{57}\text{Ni}$	+0.102
$^{36}\text{Ar}(\alpha, p)^{39}\text{K}$	+0.037
$^{44}\text{Ti}(\alpha, \gamma)^{48}\text{Cr}$	-0.024
$^{12}\text{C}(\alpha, \gamma)^{16}\text{O}$	-0.017
$^{57}\text{Ni}(p, \gamma)^{58}\text{Cu}$	+0.013
$^{58}\text{Cu}(p, \gamma)^{59}\text{Zn}$	+0.011
$^{36}\text{Ar}(\alpha, \gamma)^{40}\text{Ca}$	+0.008
$^{44}\text{Ti}(p, \gamma)^{45}\text{V}$	-0.005
$^{57}\text{Co}(p, \gamma)^{58}\text{Ni}$	+0.002
$^{57}\text{Ni}(n, \gamma)^{58}\text{Cu}$	+0.002
$^{54}\text{Fe}(\alpha, n)^{57}\text{Ni}$	+0.002
$^{40}\text{Ca}(\alpha, p)^{43}\text{Sc}$	-0.002

Table 6. Order of importance of reactions producing ^{44}Ti at $\eta=0.002$ from low multiplication factor ($0.01\times$) and high multiplication factor ($100\times$).

Rank	Reaction rate multiplied by 1/100		Reaction rate multiplied by 100	
	Reaction	% ^{44}Ti change	Reaction	% ^{44}Ti change
1	$^{44}\text{Ti}(\alpha,\text{p})^{47}\text{V}$	+208	$^{44}\text{Ti}(\alpha,\text{p})^{47}\text{V}$	-93
2	$^{12}\text{C}(\alpha,\gamma)^{16}\text{O}$	-72	$^{44}\text{Ti}(\alpha,\gamma)^{48}\text{Cr}$	-66
3	$^{40}\text{Ca}(\alpha,\gamma)^{44}\text{Ti}$	-66	$^{27}\text{Al}(\alpha,\text{n})^{30}\text{P}$	-60
4	$^{20}\text{Ne}(\alpha,\gamma)^{24}\text{Mg}$	-16	$^{30}\text{Si}(\alpha,\text{n})^{33}\text{S}$	-33
5	$^{30}\text{Si}(\text{p},\gamma)^{31}\text{P}$	-9.2	$^{12}\text{C}(\alpha,\gamma)^{16}\text{O}$	+18
6	$^{36}\text{Ar}(\alpha,\text{p})^{39}\text{K}$	-7.9	$^{40}\text{Ca}(\alpha,\gamma)^{44}\text{Ti}$	+15
7	$^{59}\text{Ni}(\text{p},\text{n})^{59}\text{Cu}$	-4.7	$^{23}\text{Na}(\alpha,\text{p})^{26}\text{Mg}$	-4.7
8	$^{59}\text{Ni}(\text{p},\gamma)^{60}\text{Cu}$	-4.7	$^{39}\text{K}(\alpha,\text{p})^{42}\text{Ca}$	+4.7
9	$^{44}\text{Ti}(\alpha,\gamma)^{48}\text{Cr}$	+2.8	$^{27}\text{Al}(\text{p},\gamma)^{28}\text{Si}$	+4.3
10	$^{27}\text{Al}(\alpha,\text{n})^{30}\text{P}$	+2.7	$^{24}\text{Mg}(\alpha,\gamma)^{28}\text{Si}$	+4.2

Table 7. Order of importance of reactions producing ^{44}Ti at $\eta=0.006$ from low multiplication factor ($0.01\times$) and high multiplication factor ($100\times$).

Rank	Reaction rate multiplied by 1/100		Reaction rate multiplied by 100	
	Reaction	% ^{44}Ti change	Reaction	% ^{44}Ti change
1	$^{44}\text{Ti}(\alpha,\text{p})^{47}\text{V}$	+211	$^{44}\text{Ti}(\alpha,\text{p})^{47}\text{V}$	-93
2	$^{12}\text{C}(\alpha,\gamma)^{16}\text{O}$	-79	$^{44}\text{Ti}(\alpha,\gamma)^{48}\text{Cr}$	-65
3	$^{40}\text{Ca}(\alpha,\gamma)^{44}\text{Ti}$	-65	$^{27}\text{Al}(\alpha,\text{n})^{30}\text{P}$	-56
4	$^{20}\text{Ne}(\alpha,\gamma)^{24}\text{Mg}$	-11	$^{30}\text{Si}(\alpha,\text{n})^{33}\text{S}$	-39
5	$^{30}\text{Si}(\text{p},\gamma)^{31}\text{P}$	-9.6	$^{12}\text{C}(\alpha,\gamma)^{16}\text{O}$	+19
6	$^{36}\text{Ar}(\alpha,\text{p})^{39}\text{K}$	-7.5	$^{40}\text{Ca}(\alpha,\gamma)^{44}\text{Ti}$	+15
7	$^{27}\text{Al}(\alpha,\text{p})^{30}\text{Si}$	-4.0	$^{58}\text{Ni}(\alpha,\gamma)^{62}\text{Zn}$	-8.7
8	$^{33}\text{S}(\text{p},\gamma)^{34}\text{Cl}$	+3.8	$^{27}\text{Al}(\text{p},\gamma)^{28}\text{Si}$	+6.0
9	$^{16}\text{O}(\alpha,\gamma)^{20}\text{Ne}$	-3.8	$^{24}\text{Mg}(\alpha,\gamma)^{28}\text{Si}$	+6.0
10	$^{30}\text{Si}(\alpha,\text{n})^{33}\text{S}$	+3.5	$^{39}\text{K}(\alpha,\text{p})^{42}\text{Ca}$	+5.3

Table 8. **Fits to thermally-averaged cross sections $N_A < \sigma v >$ (in $\text{cm}^3 \text{ s}^{-1} \text{ mole}^{-1}$) used in our calculations**

Reaction	A	B	C	D	E	F	G
$^{44}\text{Ti}(\alpha, \text{p})^{47}\text{V}$	110.00000	-3.84890	-47.13600	-91.31700	7.65930	-.54662	30.27300
$\alpha(2\alpha, \gamma)^{12}\text{C}$	CF88						
$^{45}\text{V}(\text{p}, \gamma)^{46}\text{Cr}$	90.47900	.55899	-37.67100	-57.76700	5.08410	-.31734	10.46700
$^{40}\text{Ca}(\alpha, \gamma)^{44}\text{Ti}$	119.01000	-4.29580	105.93000	-250.83000	10.96000	-.50058	128.14999
$^{57}\text{Co}(\text{p}, \text{n})^{57}\text{Ni}$	13.38000	-46.93500	-3.84000	9.20780	-.27549	.00430	-3.93210
$^{36}\text{Ar}(\alpha, \text{p})^{39}\text{K}$	63.29300	-14.78800	-29.48900	-42.76300	5.14390	-.42968	11.34400
$^{44}\text{Ti}(\alpha, \gamma)^{48}\text{Cr}$	81.02500	4.26030	-245.58000	137.92000	-2.79730	-.07990	-98.51900
$^{12}\text{C}(\alpha, \gamma)^{16}\text{O}$	1.7 × CF88						
$^{57}\text{Ni}(\text{p}, \gamma)^{58}\text{Cu}$	109.94000	-1.16540	35.84500	-155.78999	9.22410	-.50439	64.77700
$^{58}\text{Cu}(\text{p}, \gamma)^{59}\text{Zn}$	118.27000	-1.34030	45.34600	-175.61000	10.46300	-.59085	73.47000
$^{36}\text{Ar}(\alpha, \gamma)^{40}\text{Ca}$	273.35001	-5.81920	235.08000	-552.10999	34.32800	-2.01860	245.53999
$^{44}\text{Ti}(\text{p}, \gamma)^{45}\text{V}$	81.78900	.07713	-30.83200	-55.66900	5.66600	-.43928	10.56000
$^{57}\text{Co}(\text{p}, \gamma)^{58}\text{Ni}$	70.29000	-1.41470	30.19200	-105.66000	5.11650	-.27513	50.64400
$^{57}\text{Ni}(\text{n}, \gamma)^{58}\text{Cu}$	15.67600	-.01193	.42180	-.30912	.08421	-.01823	.01975
$^{54}\text{Fe}(\alpha, \text{n})^{57}\text{Ni}$	17.59100	-67.55000	1.68610	-4.90450	.88835	-.05892	1.50260
$^{40}\text{Ca}(\alpha, \text{p})^{43}\text{Sc}$	52.60400	-40.91600	-22.86600	-28.98800	1.59900	-.06980	10.16200

The rates for these reactions are from CF88 (Caughlan & Fowler 1988) or are from the formula $N_A < \sigma v > = \exp(A + B/T_9 + C/T_9^{1/3} + DT_9^{1/3} + ET_9 + FT_9^{5/3} + G \ln T_9)$.

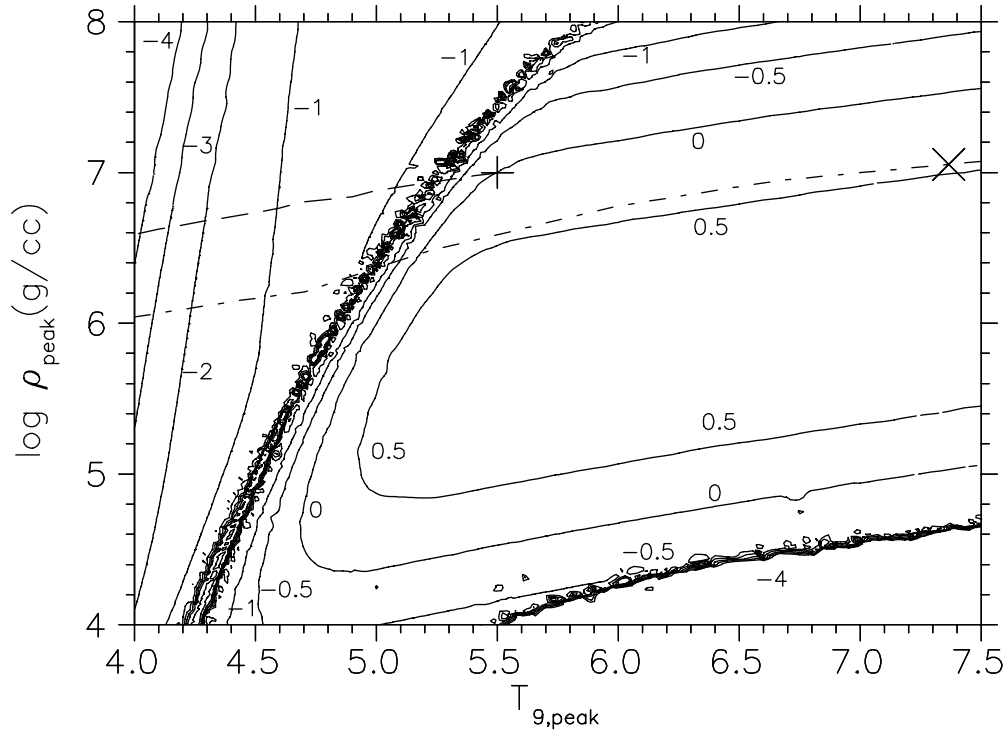


Fig. 1.— Final ^{44}Ti mass fraction in a zone expanding with $\rho \propto T^3$ as a function of initial density (g/cc) and temperature (K) for initial composition consisting of pure ^{28}Si . The contour levels show the logarithm of the final ^{44}Ti mass fractions relative to the final ^{44}Ti mass fraction in our reference calculation that began with initial temperature $T_9=5.5$ and density $\rho=10^7$ g/cc (+ sign). This figure shows that the initial temperature and density chosen for the survey in the rest of this paper (+ sign) produces a final ^{44}Ti mass fraction that is roughly equal to the final ^{44}Ti mass fraction over a quite large range of initial temperatures and densities. Most of the plane is within a factor 10. The dashed line shows the temporal evolution of temperature and density in the $\rho \propto T^3$ expansion of our survey. The dash-dotted line shows the peak temperatures and densities of matter in the ejecta of the $20 M_\odot$ supernova model of Thielemann et al. (1990). The \times sign locates the mass cut of the model at $\sim 1.6 M_\odot$ radius in order to eject $0.07 M_\odot$ of ^{56}Ni . It is important to note that unlike the dashed curve, the dash-dotted curve is not a time history of a single zone. Rather, it shows the peak conditions of ρ and T_9 reached by a continuum of mass zones in the explosion. The conditions chosen for our reference calculation are reasonably close to those achieved in supernova models. The ridge extending from the bottom left to the top middle of the figure comprises initial conditions for which the final ^{44}Ti mass fraction reaches its highest yield; this is the condition where the abundance of heavy nuclei within QSE is much the same as the abundance of heavy nuclei within NSE from the moment when quasi-equilibrium is first achieved until the freezeout.

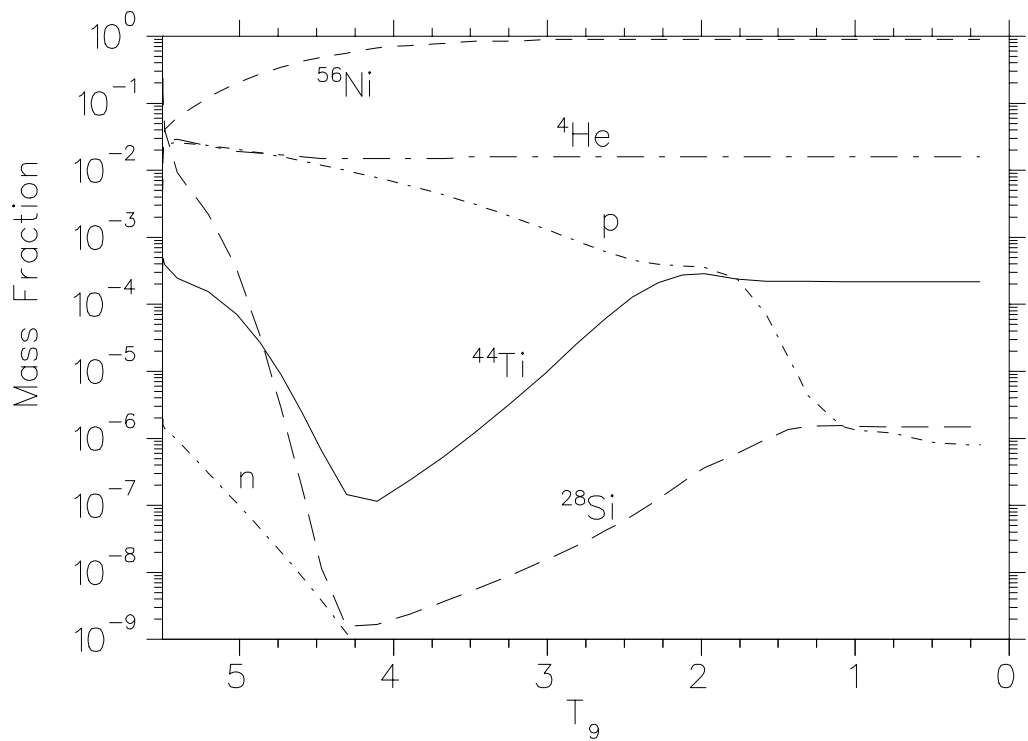


Fig. 2.— The evolution of the mass fractions of some important nuclei in the nearly adiabatic expansion experiencing alpha-rich freezeout with standard nuclear reaction rates and initial temperature $T_9=5.5$ and density $\rho=10^7$ g/cc.

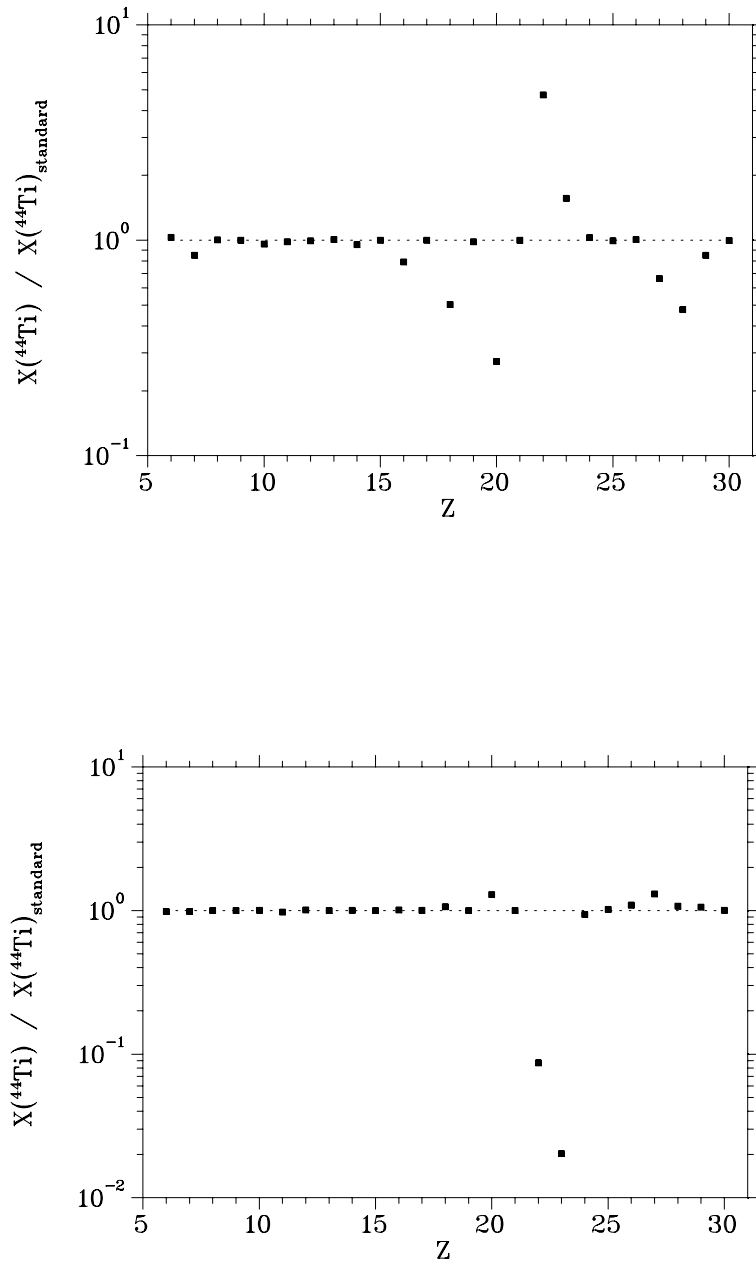


Fig. 3.— The ratio of the final ^{44}Ti mass fraction to the ^{44}Ti mass fraction from the standard network if the reaction rates of all charge-increasing and mass-increasing reactions of all isotopes of a single element are multiplied, element by element, by 0.01(a) or 100 (b).

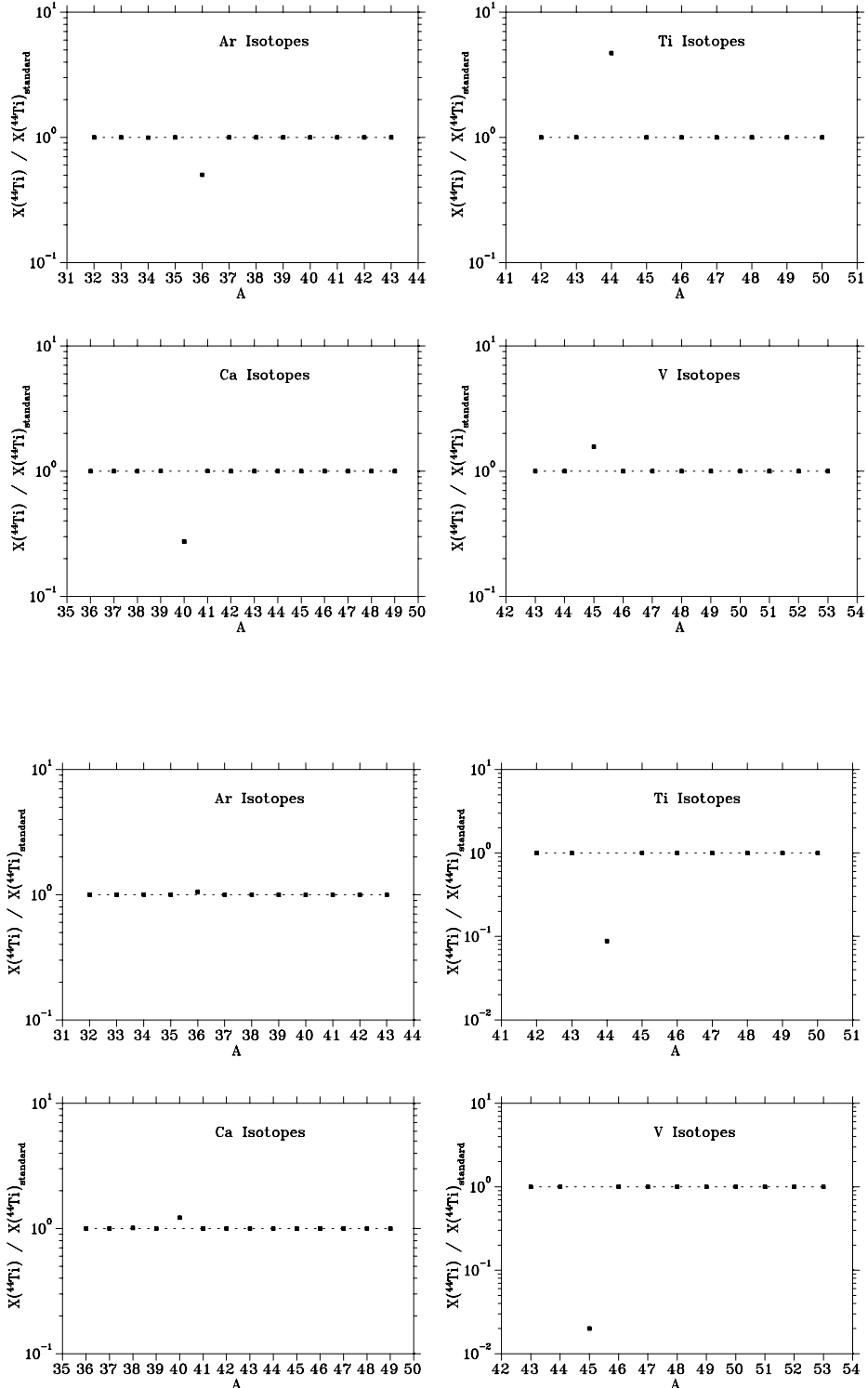


Fig. 4.— $X(^{44}\text{Ti})/X(^{44}\text{Ti})_{\text{standard}}$ for isotopic reaction rates decreased by $\times 0.01$ (a) and increased by $\times 100$ (b). Reactions with ^{44}Ti and ^{45}V produce the largest abundance sensitivity.

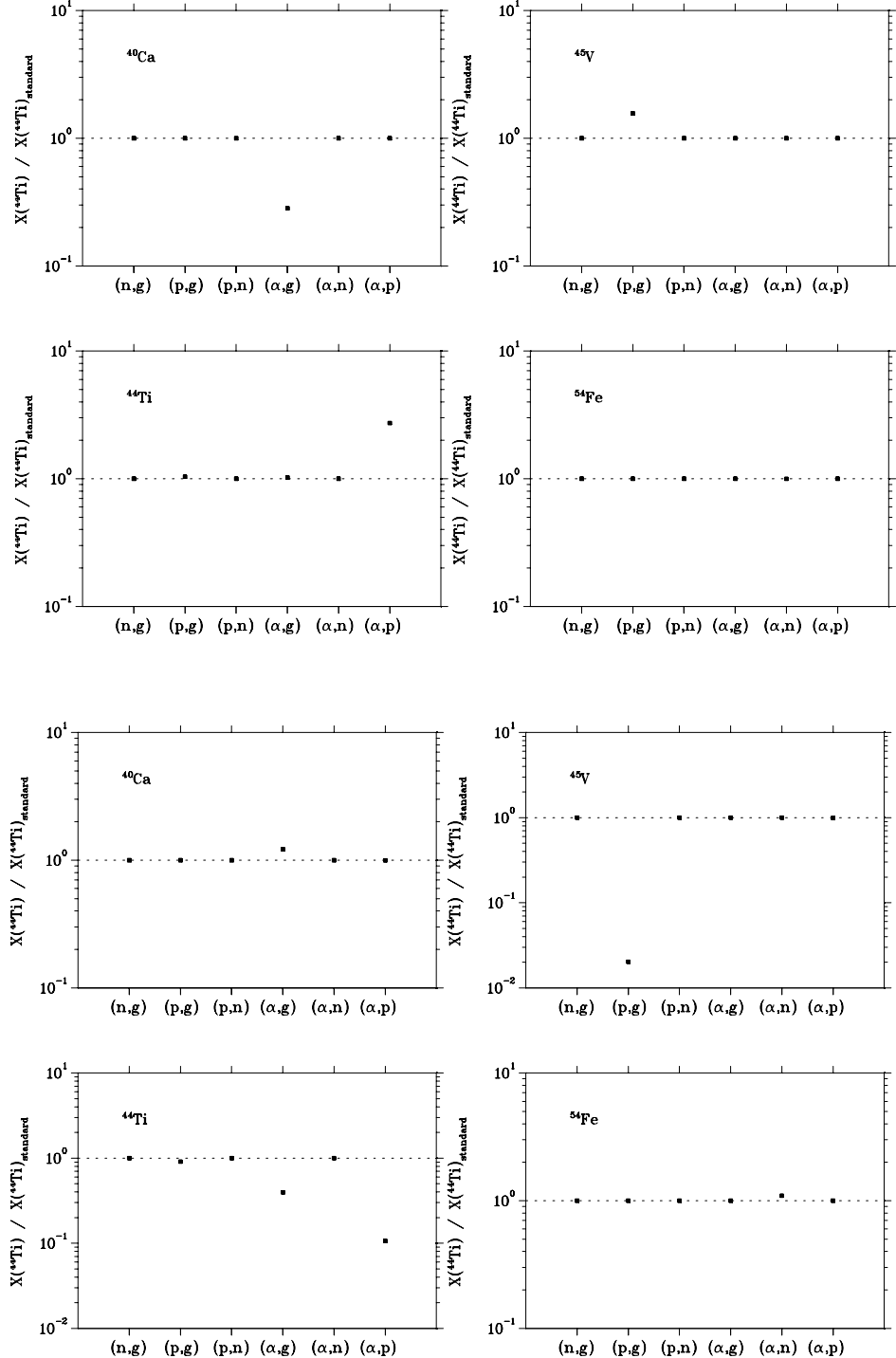


Fig. 5.— $X(^{44}\text{Ti})/X(^{44}\text{Ti})_{\text{standard}}$ for reaction rates decreased by $\times 0.01$ (top) and increased by $\times 100$ (bottom). Reactions with ^{44}Ti and ^{45}V produce the largest abundance sensitivity.

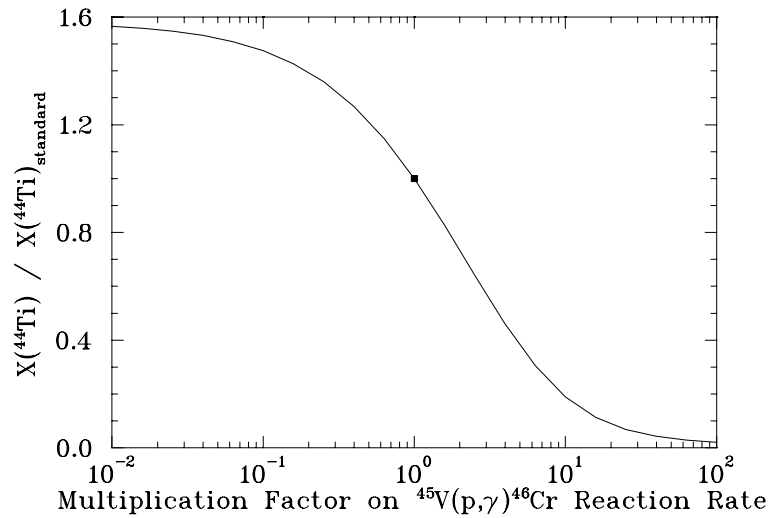


Fig. 6.— Final $X(^{44}\text{Ti})$ dependence on the reaction rate of $^{45}\text{V}(p, \gamma)^{46}\text{Cr}$.

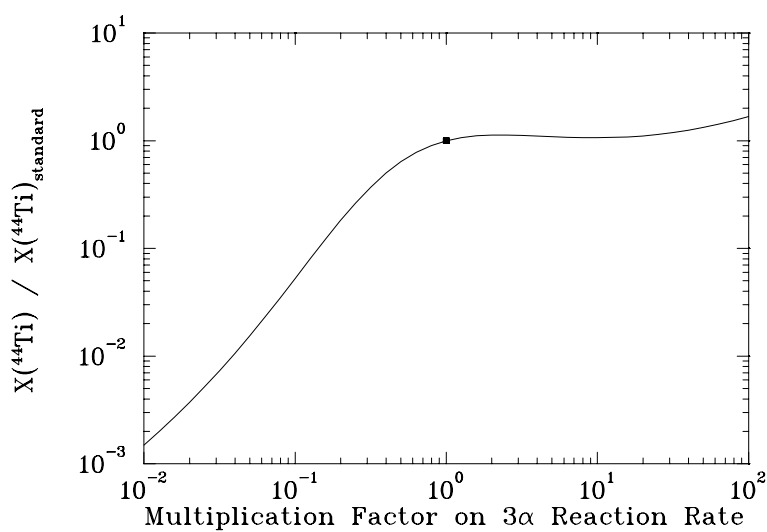


Fig. 7.— Final $X(^{44}\text{Ti})$ dependence on the reaction rate of $\alpha(2\alpha)$.

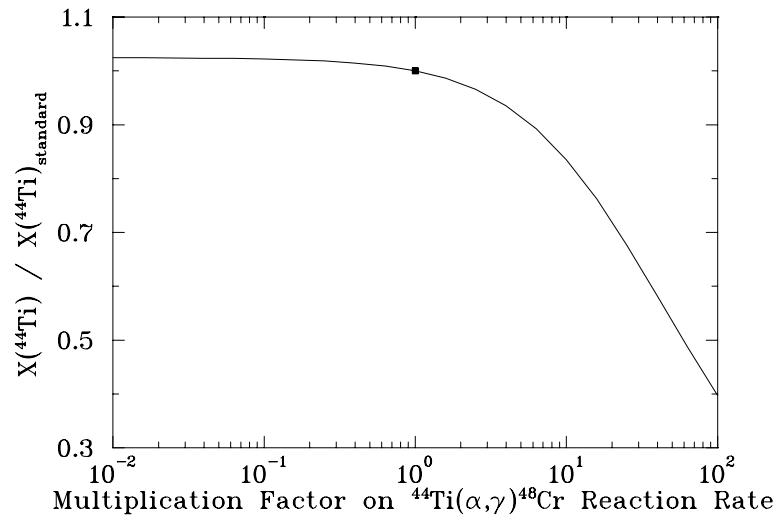


Fig. 8.— Final $X(^{44}\text{Ti})$ dependence on the reaction rate of $^{44}\text{Ti}(\alpha, \gamma)^{48}\text{Cr}$.

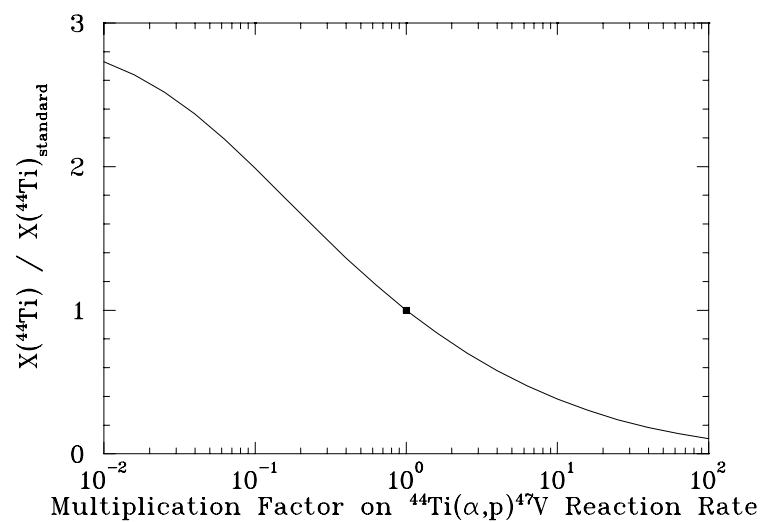


Fig. 9.— Final $X(^{44}\text{Ti})$ dependence on the reaction rate of $^{44}\text{Ti}(\alpha, p)^{47}\text{V}$.

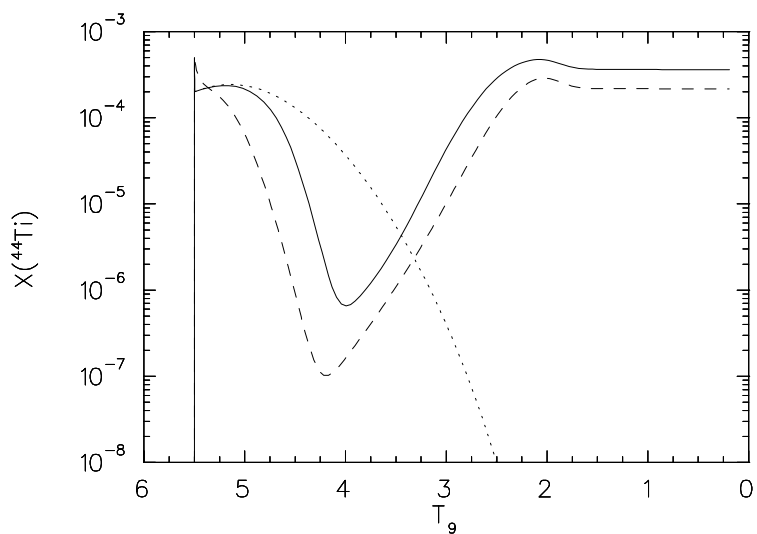


Fig. 10.— Evolution of the ^{44}Ti mass fraction as the temperature falls, with the standard triple-alpha rate (dashed curve) and also with the rate increased by $\times 100$ (solid line). The dotted line shows the NSE mass fraction of ^{44}Ti during the expansion.

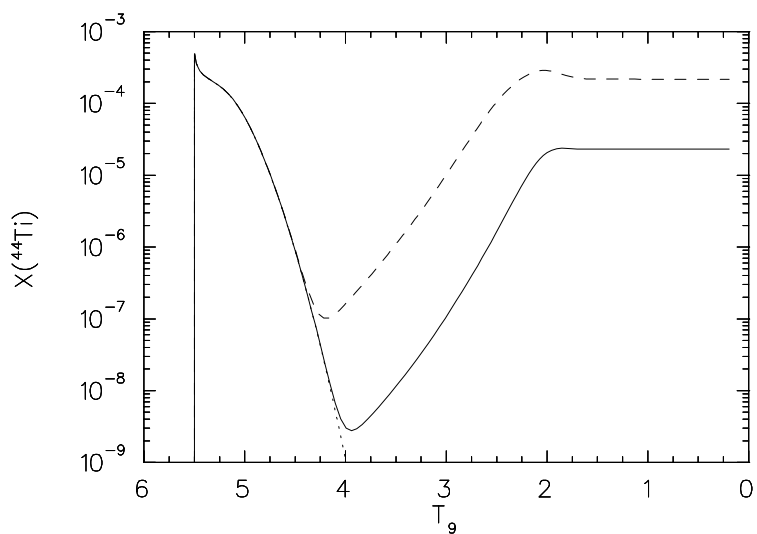


Fig. 11.— Evolution of the ^{44}Ti mass fraction as the temperature falls, with the standard $^{44}\text{Ti}(\alpha, p)^{47}\text{V}$ rate (dashed curve) and also with the rate increased by $\times 100$ (solid line). The dotted line shows the QSE mass fraction of ^{44}Ti during the expansion.

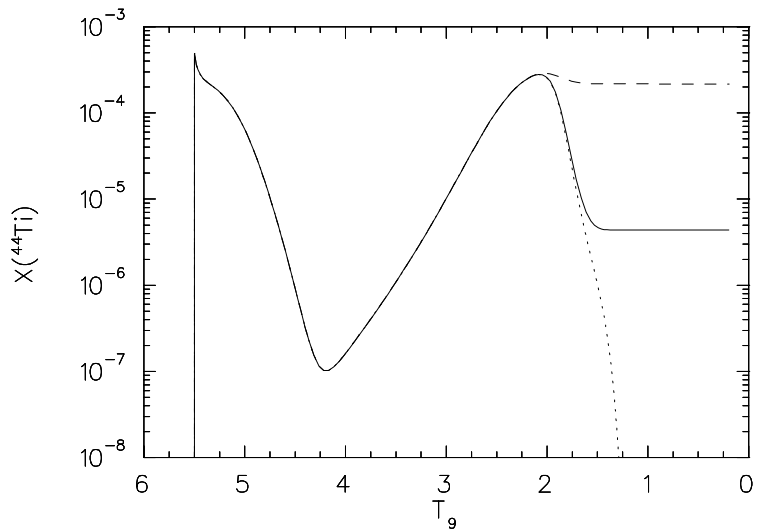


Fig. 12.— Evolution of the ^{44}Ti mass fraction as the temperature falls, with the standard $^{45}\text{V}(p, \gamma)^{46}\text{Cr}$ rate (dashed curve) and also with the rate increased by $\times 100$ (solid line). The dotted line shows the mass fraction of ^{44}Ti during the expansion if $(p, \gamma) - (\gamma, p)$ equilibrium for the $N = 22$ isotones were able to persist.

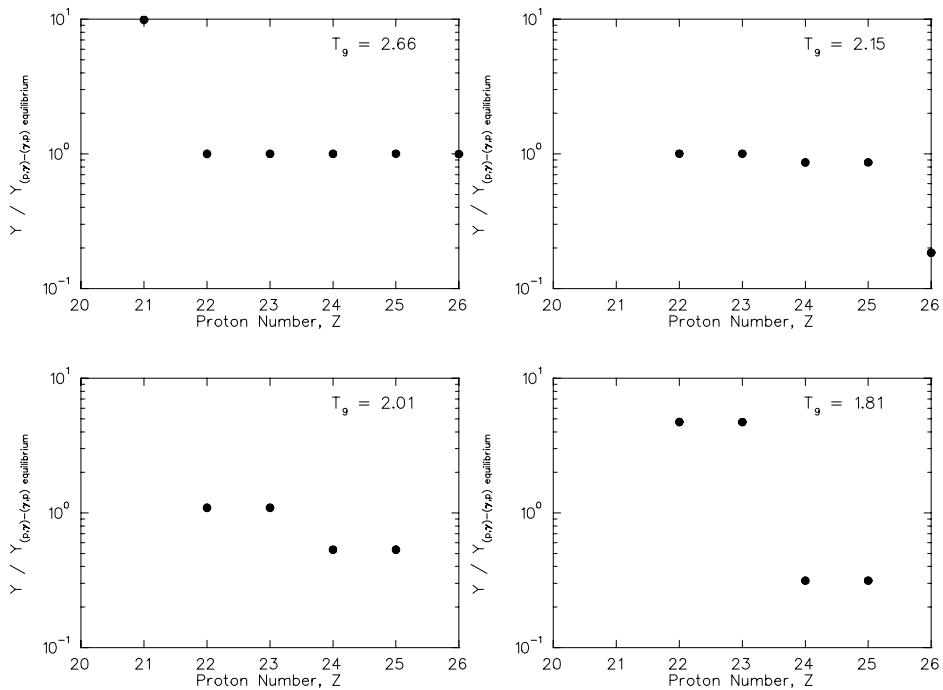


Fig. 13.— Evolution of the $(p, \gamma) - (\gamma, p)$ equilibrium for the $N=22$ isotones as the temperature falls, with the standard $^{45}\text{V}(p, \gamma)^{46}\text{Cr}$ rate. The ^{44}Ti and ^{45}V pair ($Z=22$ and 23) increasingly depart from equilibrium with the ^{46}Cr and ^{47}Mn pair ($Z=24$ and 25) as the temperature declines.

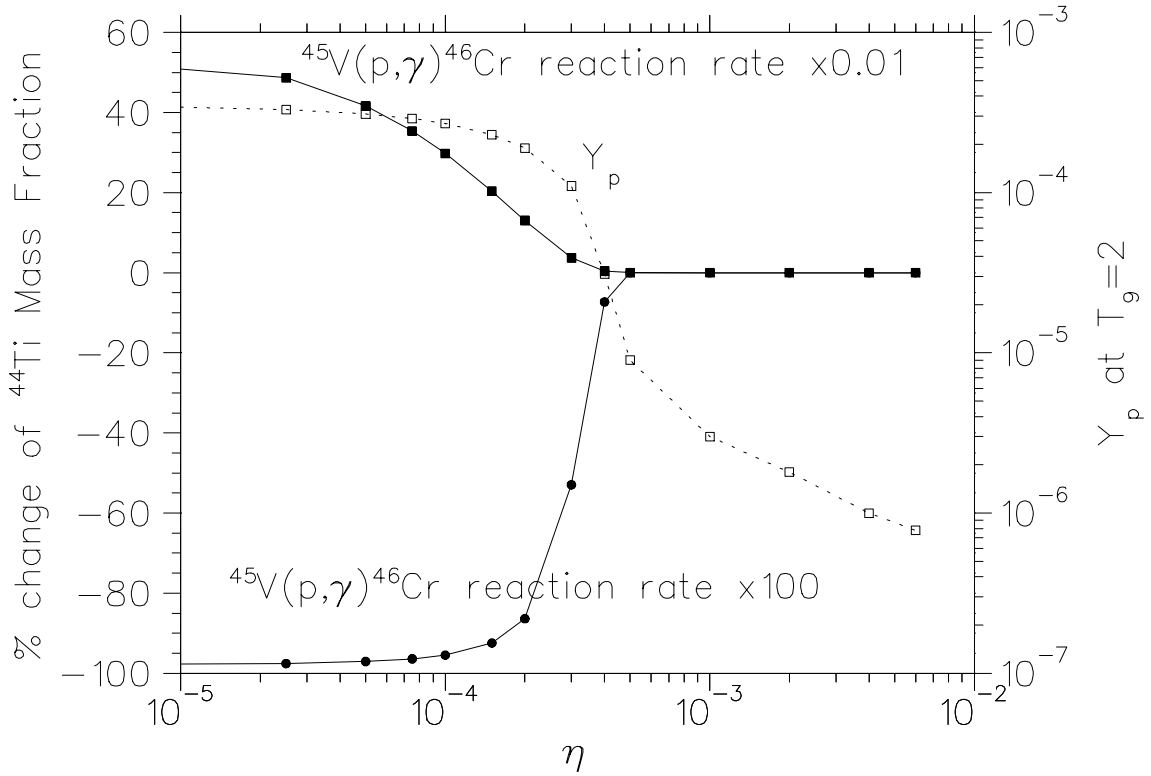


Fig. 14.— The percentage changes of ^{44}Ti mass fraction as a function of η when the standard $^{45}\text{V}(\text{p},\gamma)^{46}\text{Cr}$ reaction rate is decreased by $\times 0.01$ (filled squares) and increased by $\times 100$ (filled circles). The importance of $^{45}\text{V}(\text{p},\gamma)^{46}\text{Cr}$ reaction rate to the ^{44}Ti production in alpha-rich freezeout condition declines at $\eta \geq 0.0004$. The dotted line (open squares) shows the proton abundance at $T_9=2$ as a function of η . The drop of the proton abundance at $\eta \geq 0.0004$ causes the diminishing importance of $^{45}\text{V}(\text{p},\gamma)^{46}\text{Cr}$ reaction rate for increasing neutron richness.